



Biomass-Derived Carbonaceous Materials to Achieve High-Energy-Density Supercapacitors

Boryana Karamanova¹, Maria Shipochka², Martin Georgiev³, Toma Stankulov¹, Antonia Stoyanova¹ and Radostina Stoyanova^{2*}

¹ Institute of Electrochemistry and Energy Systems, Bulgarian Academy of Sciences, Sofia, Bulgaria, ² Institute of General and Inorganic Chemistry, Bulgarian Academy of Sciences, Sofia, Bulgaria, ³ Institute of Physical Chemistry, Bulgarian Academy of Sciences, Sofia, Bulgaria

OPEN ACCESS

Edited by:

Weigang Zhao,
Fujian Agriculture and Forestry
University, China

Reviewed by:

Kwun Nam Hui,
University of Macau, China
Francisco Carrasco-Marín,
University of Granada, Spain

*Correspondence:

Radostina Stoyanova
radstoy@svr.igic.bas.bg

Specialty section:

This article was submitted to
Carbon-Based Materials,
a section of the journal
Frontiers in Materials

Received: 17 January 2021

Accepted: 22 March 2021

Published: 16 April 2021

Citation:

Karamanova B, Shipochka M,
Georgiev M, Stankulov T,
Stoyanova A and Stoyanova R (2021)
Biomass-Derived Carbonaceous
Materials to Achieve
High-Energy-Density
Supercapacitors.
Front. Mater. 8:654841.
doi: 10.3389/fmats.2021.654841

Biomass-derived carbonaceous materials are considered as one of the most perspective electrodes for symmetric supercapacitors working with alkaline-basic electrolytes. However, they still exhibit lower energy density. Herein, we demonstrate the capacitance performance of the commercial carbon product (YP-50F, “Kuraray Europe” GmbH), obtained from coconuts, in symmetric supercapacitors by using lithium and sodium organic electrolytes. It is found that YP-50F delivers higher energy density when lithium electrolyte containing LiBF₄ salt is employed. The sodium electrolyte with NaPF₆ salt is less aggressive toward YP-50F than that of LiPF₆ salt, as a result of which a good capacitance performance is observed in the sodium electrolyte. The contributions of surface functional groups of YP-50F, as well as its compatibility with non-aqueous lithium and sodium electrolyte, are discussed on the basis of *post-mortem* scanning electron microscopy (SEM)/energy-dispersive X-ray spectroscopy (EDS) and X-ray photoelectron spectroscopy (XPS) data analyses. The obtained correlations could be of significance in order to design sustainable supercapacitors with high energy density.

Keywords: biomass carbonaceous materials, symmetric supercapacitors, organic lithium and sodium electrolytes, *post-mortem* analysis, electrode/electrolyte interactions

INTRODUCTION

The rapidly growing portable electronics market in the last years has evoked a high demand for better energy storage devices with high power density (Simon and Gogotsi, 2008; Etacheri et al., 2011). The electrochemical supercapacitors (ESs) satisfy these requirements to a great extent, but the relatively low energy density limits their future applications (Simon and Gogotsi, 2008). The energy storage in supercapacitors includes reversible reactions of electrostatic adsorption/desorption of electrolyte ions on the charged electrode surface (i.e., electrical double-layer capacitance) (Simon and Gogotsi, 2008; Etacheri et al., 2011). The energy density depends on the right choice of electrode materials, as well as on their compatibility with electrolyte ions. Because of extremely high specific surface area, abundantly availability, and low cost, activated carbons obtained from biomass are widely employed as electrodes in supercapacitors (Rufford et al., 2008; Bi et al., 2019). The advantages of biomass-derived carbons over others are the presence of

diverse functional groups contributing to the extra charge storage in supercapacitors due to their participation in pseudocapacitance redox reactions (Bi et al., 2019). Recently, we have demonstrated that commercial coconut-derived carbons, possessing high amount of acidic groups and narrow pore size distribution, display excellent cycling stability in an alkaline electrolyte solution: the discharge capacitance decreases by only a 2% after 37,000 cycles (Karamanova et al., 2019, 2020).

The used electrolyte is the other key component of ESs, providing ionic conductivity and thus favoring the charge compensation on the electrodes in the cell (Zhong et al., 2015). The desirable properties of electrolytes are high ionic conductivity, wide voltage window, high electrochemical and thermal stability, low viscosity, low toxicity, low cost, etc. (Wang et al., 2012). The electrolyte evaluation shows that the higher power density is achieved by aqueous electrolytes, while the organic electrolytes are more suitable to reaching higher energy density (Calvo et al., 2014). Such finding is a consequence of the fact that the operating voltage window is wider in organic electrolytes (Phattharasupakun et al., 2017).

The various performances of biomass-derived carbons in aqueous and non-aqueous electrolytes are usually related with ionic conductivity and electrolyte ion size, as well as with the interaction between the electrolyte and the electrode materials (Chen et al., 2019). In this case, the matching between the electrolyte ion size and the pore size of carbon electrode material has a profound impact on the achievable specific capacitance (Yang et al., 2007; McDonough et al., 2012). For example, the presence of very small pores in a carbon material may increase the specific surface area, but it can also limit the accessibility of electrolyte ions. Especially, the larger organic ions cannot easily get access with the small pores, resulting in a negative effect on specific capacitance (Chmiola et al., 2006).

The compatibility of the electrolyte and activated carbon contributes to the operating voltage of supercapacitors. The frequently used organic electrolytes (especially for commercial ESs) are the solution of the tetraethylammonium tetrafluoroborate (TEABF₄) in the acetonitrile (ACN) or propylene carbonate (PC) solvent (Rufford et al., 2008). In addition, battery-like electrolytes such as 1M LiPF₆ in ethylene carbonate (EC)/dimethyl carbonate (DMC) or in EC/ethyl methyl carbonate (EMC)/DMC, as well as 1 M NaPF₆ in EC–DMC–PC–EA, are also utilized (Qian et al., 2014; Vali et al., 2014; Yue et al., 2020). However, one should take into account that the addition of EC leads to the lowering of the electrochemical stability of electrolytes, especially at lower voltages (Yue et al., 2020). Because of the different storage mechanism, the electrolyte stability in batteries and supercapacitors varies significantly irrespective of their similar composition: while the decomposition voltage of LiPF₆/(EC+EMC+DMC) in lithium-ion cells is higher than 4 V; the same electrolyte is decomposed in supercapacitor cells above 3.0 V (Pasquier et al., 2004; Hu et al., 2009). All the above features indicate that organic electrolytes are a powerful tool to increase the energy density of ESs. Despite the variety of experimental data, the role of the organic electrolyte on the supercapacitor performance is still under debate.

Herein, we demonstrate the role of the lithium and sodium non-aqueous electrolytes to achieve high energy density of symmetric supercapacitors based on commercial biomass-derived carbons. As electrolytes, we used 1M LiBF₄ and 1M LiPF₆ solutions in ethylene carbonate/dimethyl carbonate (EC/DMC = 1:1), as well as 1M NaPF₆ in PC. Both LiPF₆ and NaPF₆ electrolytes are characterized with high ionic conductivity in comparison with the LiBF₄ electrolyte (Ponrouch et al., 2015; Li et al., 2016). As biomass-derived carbons, commercial product YP-50F (“Kuraray Europe” GmbH) obtained from coconuts is employed. These products, possessing a high amount of acidic functional groups and narrow pore size distribution, are subjects of the study since they show magnificent cycling stability in aqueous LiOH and NaOH electrolytes (Karamanova et al., 2020). The interaction between the biomass-derived carbon electrodes and the organic electrolyte is examined on the basis of *post-mortem* scanning electron microscopy (SEM)/energy-dispersive x-ray spectroscopy (EDS) and x-ray photoelectron spectroscopy (XPS) analyses of the electrodes after cell cycling.

EXPERIMENTAL SECTION

The commercial activated carbon (YP-50F, “Kuraray Europe” GmbH) was used to fabricate electrodes for supercapacitor cells. The electrodes were composed from a mixture of 80 wt.% YP-50F, 10 wt.% graphite ABG 1005 EG-1, and 10 wt.% polyvinylidene difluoride (PVDF) binder. The electrodes were dried in vacuum at 80°C for 12 h and pressed under pressure of 20 MPa. The obtained electrodes were mounted in the electrochemical cell with a Whatman separator and filled with the electrolyte in a dry box under argon atmosphere. The reference electrode was Li/Li⁺ or Na/Na⁺. The symmetric supercapacitor cell was assembled from two identical electrodes and three types of organic electrolytes: 1M LiBF₄ and 1M LiPF₆ in EC/DMC and 1M NaPF₆ in PC. All measurements were performed at room temperature.

The cyclic voltammetry (CV) measurements were carried out in a three-electrode cell, in a voltage window up to 3.6 V and a scan rate varying from 1 up to 100 mVs⁻¹. The CV experiments were recorded on PAR Potentiostat/Galvanostat (United States) and Multi PalmSens system (model 4, The Netherlands). The galvanostatic charge–discharge cycling tests were conducted in a two-electrode cell at constant current mode and current load varying from 60 up to 600 mA g⁻¹ for 25 cycles per step. All measurements were performed on Arbin Instrument System BT-2000 (United States). The specific capacitance was calculated from cyclic voltammograms and charge–discharge curves as described elsewhere (Karamanova et al., 2019, 2020).

The surface and morphology changes in the carbon-based electrodes during supercapacitor testing were analyzed by means of *ex-situ* SEM/EDS and XPS techniques. The XPS spectra were registered using AXIS Supra electron spectrometer (Kratos Analytical Ltd., United Kingdom) and achromatic AlK α radiation with photon energy of 1486.6 eV and charge neutralization system. The binding energies (BEs) were determined with an accuracy of ± 0.1 eV. The chemical composition in the depth of

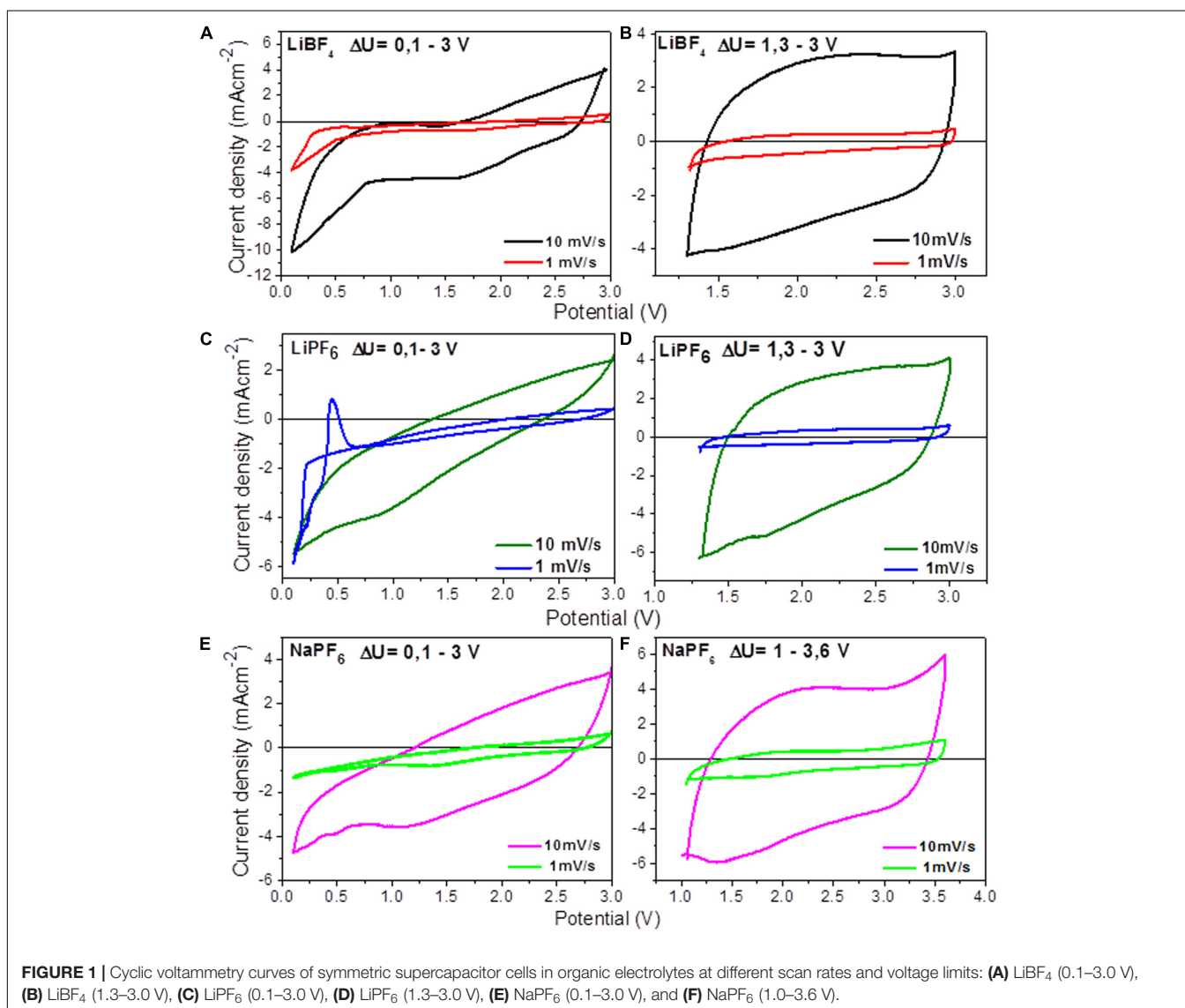
the films was determined by monitoring the areas and BEs of C1s, O1s, and F1s photoelectron peaks. Using the commercial data-processing software of Kratos Analytical Ltd., the concentrations of the different chemical elements (in atomic %) were calculated by normalizing the areas of the photoelectron peaks to their relative sensitivity factors.

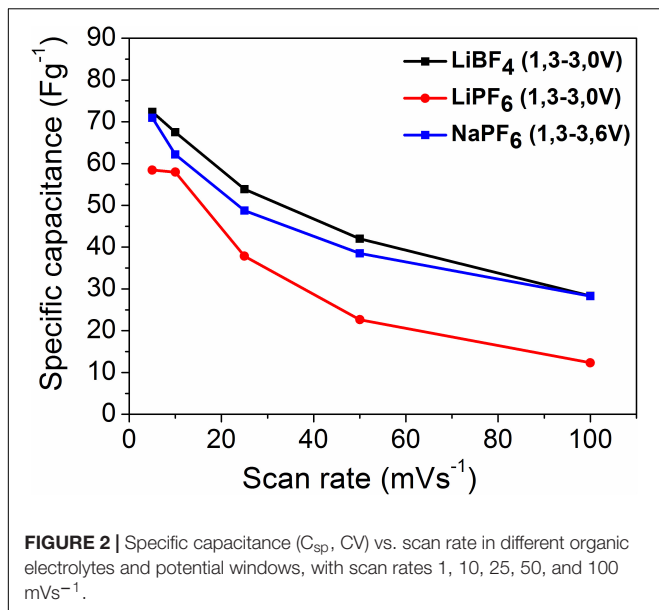
The wetting angle is measured on an apparatus, Force Tensiometer K100 of KRÜSS K100 (Germany). The measurement consists of dropping of 6.3 μl of the electrolyte on the electrode, and the obtained value of the wetting angle is averaged from five measurements.

RESULTS AND DISCUSSION

Figure 1 compares the CV curves of YP-50F cycling in lithium and sodium electrolytes. In general, all CV curves are typical for symmetric supercapacitor systems. However, some additional

features need to be discussed. The CV curves in the LiPF_6 -based electrolyte display an abrupt peak at low scan rates at 0.50/0.15 V vs. Li/Li^+ . This peak can be assigned to the interaction of Li^+ with the Al collector (Hudak and Huber, 2011). This is a specific property of Al in the LiPF_6 -based electrolyte, which is not observed in sodium electrolytes (**Figure 1**). In LiBF_4 electrolyte and below 0.5 V, there is a strong deviation of the CV curve profiles from the rectangular shape, thus indicating the contribution of parasitic redox interaction of Li^+ with YP-50F and/or interaction of Li^+ with the Al collector. At high scan rates, the effect of redox peaks on the CV curve profiles is negligible, and all CV curves bring the features of the capacitive behavior. In order to minimize the effect of the Al collector, insets in the same figure show CV curves when the low voltage limit is above 1.0 V. In this case, the capacitive behavior is better pronounced in the CV curve profiles, which look similar to a rectangle. The comparison of CV curve profiles of YP-50F reveals that the optimal voltage limits depend on the electrolyte composition:





for LiPF₆-based electrolyte, the range is of 1.2–3.4 V vs. Li/Li⁺; 1.3–3.0 V vs. Li/Li⁺ for LiBF₄; and 1.0–3.6 V vs. Na/Na⁺ in NaPF₆-based electrolytes.

From the CV curves, the specific capacitance ($C_{sp, CV}$) of YP-50F is calculated using Equation (1):

$$C_{sp, CV} = \frac{Q}{\Delta V \cdot \frac{dv}{dt} \cdot m} \quad (1)$$

where Q is the area under the CV curve, dv/dt is the scan rate, ΔV is potential window, and m is the mass of active material. The calculated capacitance values as a function of the scan rate are given in **Figure 2**.

The YP-50F exhibits higher capacitance in the LiBF₄-based electrolyte in comparison with that in LiPF₆. The capacitance of YP-50F in the sodium electrolyte approaches to that in the LiBF₄-based electrolyte. It is worth mentioning that in the sodium electrolyte, the voltage range is broader than that in the lithium electrolyte, which contributes to the energy density of the supercapacitor.

The galvanostatic charge–discharge tests are carried out in order to differentiate, further, the performance of YP-50F in lithium and sodium electrolytes. The specific capacitances are calculated according to the following equation (Wang et al., 2017):

$$C = (I \times \Delta t) / (m \times \Delta V) \quad (2)$$

where I, Δt , m, and ΔV indicate discharge current, discharge time, mass of active material, and voltage window.

The calculated capacitance of YP-50F and its dependence on the current load are shown in **Figure 3**. There are several points that need to be outlined. First, the specific capacitance decreases with the increase of the current density, probably because of the remarkable gain of the diffusion limitation inside

pore channels (Wang et al., 2015). The rate dependence seems similar for both lithium and sodium electrolytes when a broad voltage window is used (between 0.1 and 3.0 V). In the narrow voltage window (i.e., between 0.6 and 2.4 V for lithium electrolyte and between 0.1 and 2.6 V for sodium electrolyte), the rate capability of YP-50F is improved significantly. The obtained capacitance values for YP-50F in lithium and sodium organic electrolytes are lower than those in aqueous electrolytes (i.e., 6 M LiOH and 6 M NaOH) (Karamanova et al., 2020): at a current load of 60 mA/g the capacitance is about 80 F/g in LiBF₄ and NaPF₆ vs. 113 F/g and 108 F/g in LiOH and NaOH, respectively. It should be taken into account that these capacitance values are reached in different voltage window: 1.8 V for LiPF₆ and LiBF₄, 2.5 V for NaPF₆ and 1.2 V for aqueous electrolytes. This has an effect on the energy density, which is discussed below:

Among the organic electrolytes, at low current density, YP-50F cycled in LiBF₄ exhibits a higher capacitance than that of YP-50F in LiPF₆. At high current density, this trend is changing—the capacitances of YP-50F in LiBF₄ and LiPF₆ electrolytes are nearly similar (**Figure 3A**). Replacement of lithium with the sodium electrolyte does not change significantly the capacitance of YP-50F at low current load. By increasing the current load, the capacitance of YP-50F in NaPF₆ decreases more quickly than that of YP-50F in the lithium electrolyte. This means that in NaPF₆ electrolyte, YP-50F displays worse rate capability. The observed phenomenon can be related with different ionic sizes of Na⁺ than Li⁺ and their compatibility with the pore size of YP-50F. Based on first-principles molecular dynamics simulations, it has been calculated that the sizes of the first solvation shell of alkali ions in the EC solvent increase from Li⁺ to Na⁺, that is, 1.95–2.34 Å (Cresce et al., 2017). The pore sizes of YP-50F are higher than 1 nm (Karamanova et al., 2019, 2020), which means that they are accessible by solvated Li⁺ and Na⁺ ions. On the other hand, the bigger size of solvated Na⁺ ions can be related with a worse rate capability of YP-50F in the NaPF₆ electrolyte.

The cycling stability is also different when YP-50F is cycled in lithium and sodium electrolytes (**Figure 3**). After 1,000 cycles, YP-50F is characterized by highest cycling stability when the LiBF₄ electrolyte is used (i.e., about 89%). The worse cycling stability is observed for YP-50F cycled in LiPF₆-based electrolyte (i.e., about 83%). In the NaPF₆ electrolyte, the cycling stability of YP-50F varies around 84%, and it is lower than that in the LiBF₄ electrolyte. It is noticeable that, in the aqueous electrolytes, the cycling stability of YP-50F is also worse in the sodium electrolyte than in the lithium electrolyte (i.e., 91–92% in NaOH vs. 94% in LiOH) (Karamanova et al., 2020). In addition, the Columbic efficiency in both aqueous and non-aqueous electrolytes is around 99–100%. This implies that the ionic conductivity of the electrolyte and ionic sizes of Li⁺ and Na⁺ are not the only factors contributing to the supercapacitor performance.

The next factor is the wettability of the electrode by the electrolyte. Therefore, the wettability of YP-50F by organic and aqueous electrolytes (determined by the contact angle) is listed in **Table 1**. In general, the organic electrolytes wet YP-50F better in

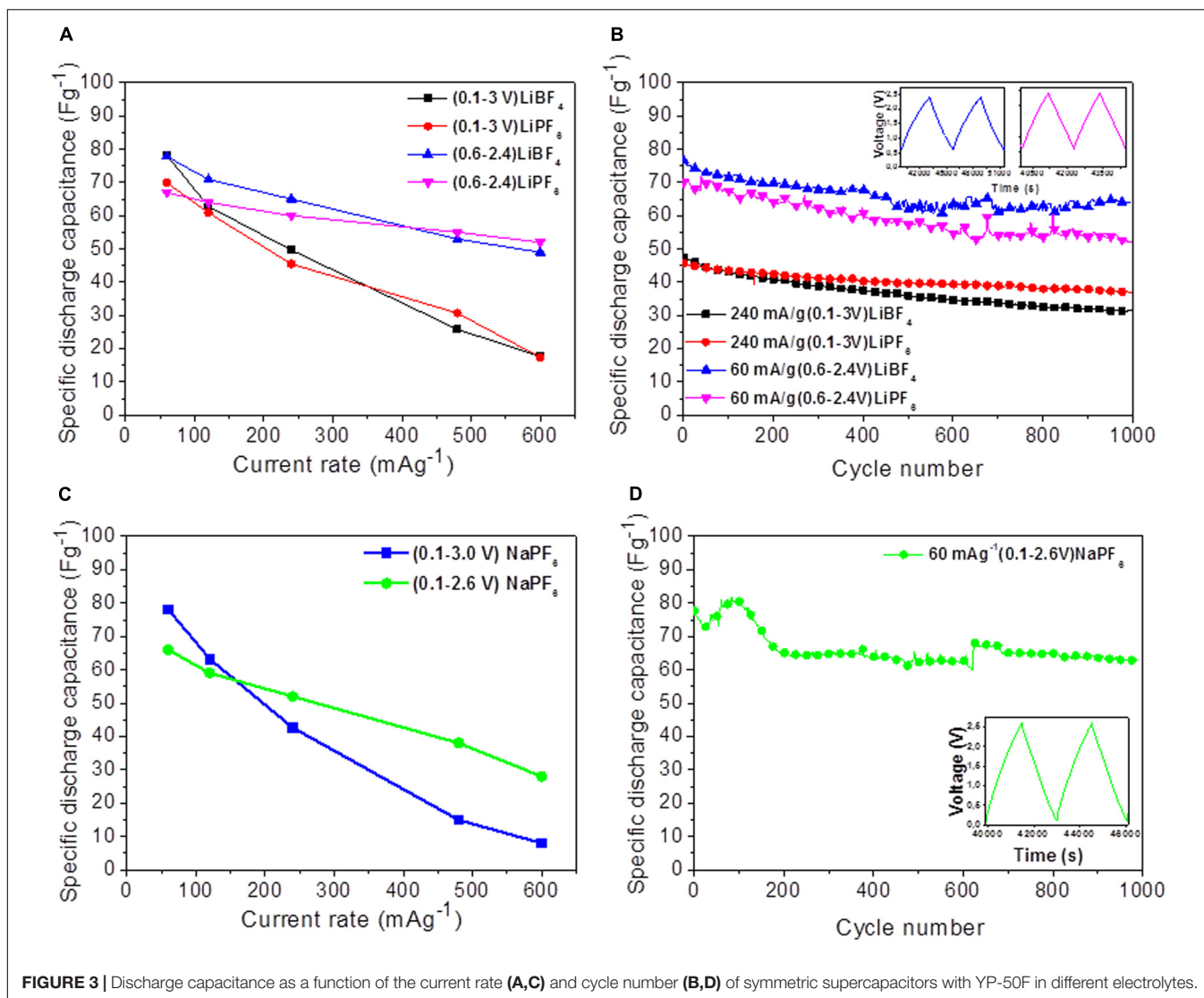


FIGURE 3 | Discharge capacitance as a function of the current rate (A,C) and cycle number (B,D) of symmetric supercapacitors with YP-50F in different electrolytes.

comparison with aqueous electrolytes. Whether it is an aqueous or an organic electrolyte, the wettability of YP-50F is better in the lithium electrolyte, especially in LiBF_4 . This can be related with an improved performance of YP-50F in the LiBF_4 electrolyte.

To get insight into the effect of the electrolyte on the supercapacitor performance, *ex-situ* SEM and XPS measurements are undertaken. For the purpose of this study, the electrodes are analyzed after CV measurements.

The SEM images of the pristine and cycled electrodes are compared in **Figure 4**. The comparison shows that the pristine electrode morphology, consisting of relatively homogeneous and dense bound particles, is maintained to a high extent when YP-50F is cycled in the LiBF_4 electrolyte.

The morphology of the electrode undergoes a significant change in the LiPF_6 electrolyte: there are micrometric cracks, and the electrode roughness seems to have increased after cell cycling. This indicates that LiPF_6 salt is more aggressive toward YP-50F than LiBF_4 . In NaPF_6 electrolyte, the changes in morphology are intermediate between that for LiBF_4 and LiPF_6 electrolytes: the cracks appear, but they are less obvious in comparison with LiPF_6 . This is experimental evidence for low chemical activity of the NaPF_6 electrolyte toward YP-50F in symmetric supercapacitors than that of the LiPF_6 electrolyte. The chemical inertness of LiBF_4 toward YP-50F, as well as an excellent wettability of YP-50F, has a major impact on the improved supercapacitor performance. The better

TABLE 1 | Contact angles of the carbon electrodes in aqueous and non-aqueous lithium and sodium electrolytes.

Electrolyte	1M LiBF_4 in EC/DMC	1M LiPF_6 in EC/DMC	1M NaPF_6 in PC	6M LiOH	6M NaOH
Contact angle, °	0° (absorbs immediately)	18.4°	38.8°	60.8°	83.7°

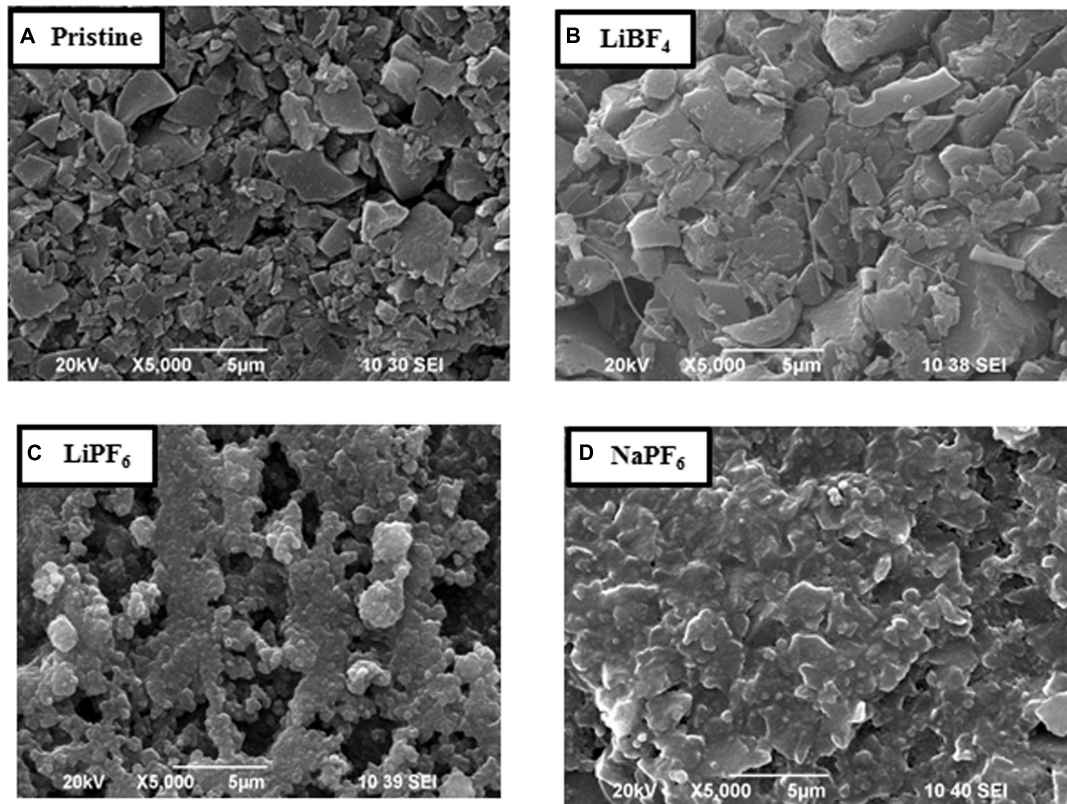


FIGURE 4 | Scanning electron microscopy images of the pristine AC electrode (A), AC electrode after CV test in the LiBF₄ electrolyte (B), LiPF₆ electrolyte (C), and NaPF₆ electrolyte (D).

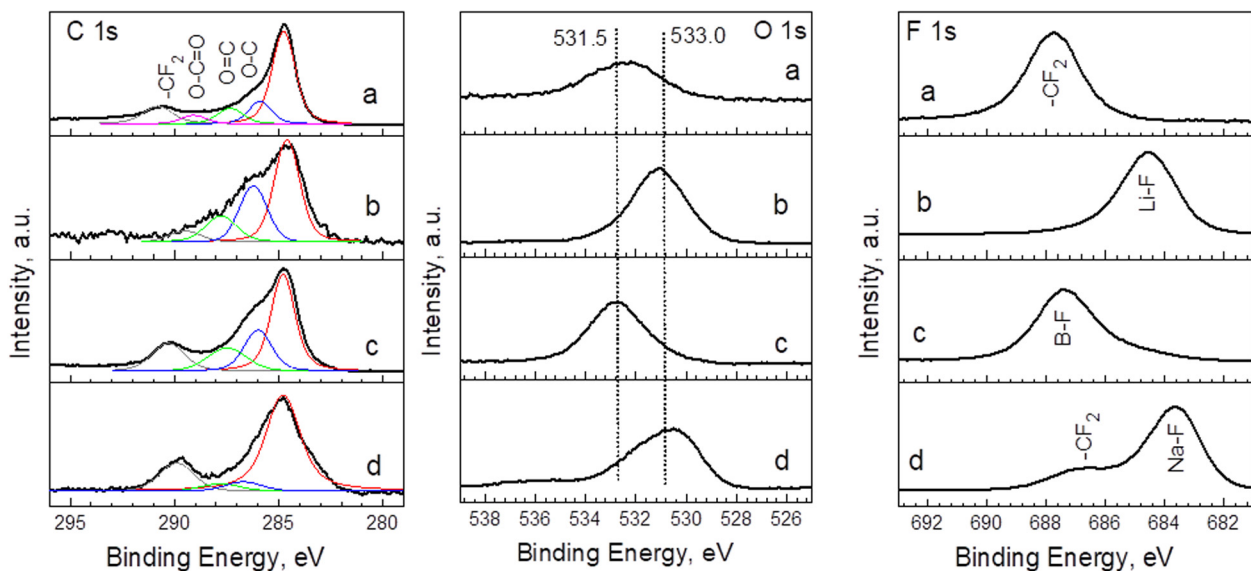


FIGURE 5 | C1s, O1s, and F1s spectra for pristine YP-50F (a) and YP-50F worked in LiPF₆ (b), LiBF₄ (c), and NaPF₆ (d) and electrolytes.

compatibility of LiBF₄ with activated carbon could be compared with recent findings of Metzger et al. (2020) on the high-voltage stability of conductive carbon with various lithium

salt (Metzger et al., 2020). Using on-line electrochemical mass spectrometry, it has been demonstrated that the LiBF₄ salt has better stability toward conductive carbon (even at 50°C) than

the LiPF_6 salt (Metzger et al., 2020). This finding concerning conductive carbon is in agreement with our observation in regard to activated carbon.

Other parameters that could contribute to the capacitance of YP-50F are the functional groups. Recently, it has been demonstrated that YP-50F exhibits predominately basic functional groups (Karamanova et al., 2019, 2020). In addition, acidic groups such as phenolic, carboxylic, and lactone groups occur in low amounts (Karamanova et al., 2019). During cycling in alkaline electrolyte, the surface of YP-50F becomes rich in carboxylic groups (Karamanova et al., 2019, 2020). In general, the carboxyl and hydroxyl groups are deprotonated in alkaline media, while the carbonyl groups participate in redox reactions and give rise to the pseudocapacitance of carbonaceous materials (Frackowiak and Beguin, 2001; Fang et al., 2012). It is worth mentioning that there are many works on the chemical reactivity of functional groups in aqueous electrolyte, but in organic electrolytes, the works are scarce. In this study, we examine the behavior of functional groups of YP-50F in organic lithium and sodium electrolytes by means of XPS spectroscopy (Figure 5). The C1s spectrum of pristine YP-50F consists of an intensive peak at 284.8 eV, which comes from sp^2 -hybridized graphitic carbon. In addition, low intensive peaks at 285.5, 287.0, and 288.8 eV can be deconvoluted. These peaks are associated with C atoms that are bonded to oxygens in hydroxyl/epoxide groups (C-O), carbonyl groups (C=O), and carboxyl groups (COOH). These assignments are also supported by O1s spectrum of pristine YP-50F. However, it should be taken into account that the assignments of O1s peaks to O species in the literature are not the straightforward procedure as in the case of C 1 spectra (Clark and Dilks, 1979; Kundu et al., 2008). Irrespective of this uncertainty, the O1s spectrum displays two overlapped peaks at 531.5 and 533.0 eV that can be assigned to double-bonded O atoms in esters, carbonates, and acids, as well as to single-bonded O atoms in ketones, ethers, and alcohols.

The cycling of YP-50F in LiPF_6 and LiBF_4 electrolytes leads to enrichments of the electrode surface with hydroxyl/epoxide groups (C-O) and carbonyl groups (C=O). This behavior of functional groups is opposite to that observed in aqueous lithium electrolyte (i.e., 6M LiOH), where the relative amount of carboxylic groups increases significantly. In comparison with lithium electrolytes, the NaPF_6 electrolyte does not provoke any significant interactions with functional groups, which are demonstrated by the C1s and O1s spectra. The new feature here is demonstrated by the F1s spectrum. There is a peak at 683.6 eV, which is due to F atoms in NaF. The fluorides are also observed on the surface of YP-50F cycled in LiPF_6 . In contrast, the surface of YP-50F is free from fluorides in the LiBF_4 electrolyte. This result can be related with higher stability of LiBF_4 in comparison with LiPF_6 and NaPF_6 .

The element amounts in pristine and worked electrodes are determined by XPS and SEM/EDS. The combined use of these two methods allows extraction of quantitative information on the chemical elements at different depth from samples: XPS provides chemical information about the few top surface layers only (i.e., up to 5 nm), while the SEM goes deeper (i.e., more than 1,000 deeper than the XPS) (Table 2).

The XPS and SEM-EDS data show that the oxygen amount is nearly homogeneously distributed over the depth of pristine YP-50F. After electrochemical reaction, the surface becomes richer on oxygen and fluorine atoms. It is of importance that the electrode surface is the poorest of O, F, and Li atoms when YP-50F worked in the LiBF_4 electrolyte. At this electrolyte, YP-50F possesses a higher capacitance performance.

The advantage of using organic electrolytes is demonstrated by the relationship between energy density and power density of the supercapacitors (SCs) (Ragone plots, Figure 6). At power density of 100 Wkg^{-1} , the SC working in LiBF_4 shows energy density of 91.1 Whkg^{-1} , which is higher in comparison with that for LiPF_6 and NaPF_6 electrolytes. It is of importance that the energy density of supercapacitors with organic electrolytes is comparable and, in some cases, higher than those previously reported (Mak et al., 2012; Zhong et al., 2015; Pazhamalai et al., 2019). The energy density in the organic electrolyte is three–four times higher than that in LiOH and NaOH electrolytes (i.e., at power density 100 Wkg^{-1} its energy density is around 21–22 Whkg^{-1}). Among organic electrolytes, YP-50F worked in the NaPF_6 electrolyte shows a very good relation between energy and power density, which will be of significance to construct a sustainable supercapacitor.

TABLE 2 | Element content (at. %) for YP-50F determined from XPS and SEM/EDS analysis for pristine and worked electrodes in different electrolytes after CV-tests.

Samples	C, at. %	O, at. %	F, at. %	P, at. %	Me, at. %
Pristine (XPS)	81.10	5.50	13.40	–	–
Pristine (SEM)	86.00	7.60	6.40	–	–
LiPF_6 (XPS)	9.70	16.90	45.30	2.60	25.50 (Li)
LiPF_6 (SEM)	29.70	12.25	57.00	1.05	–
NaPF_6 (XPS)	22.40	14.30	56.60	2.50	4.20 (Na)
NaPF_6 (SEM)	60.40	11.60	25.50	0.40	2.10 (Na)
LiBF_4 (XPS)	63.20	12.90	20.70	–	3.20 (Li)
LiBF_4 (SEM)	70.81	17.00	12.19	–	–

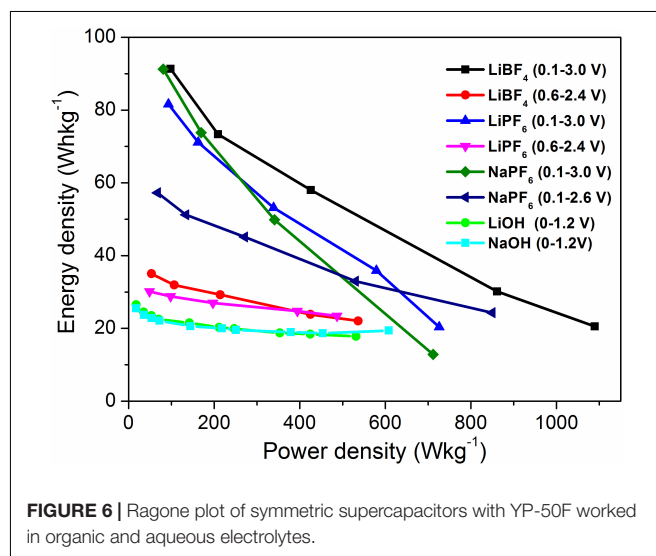


FIGURE 6 | Ragone plot of symmetric supercapacitors with YP-50F worked in organic and aqueous electrolytes.

CONCLUSION

The present study shows the capacitance performance of the commercial carbon product (YP-50F, “Kuraray Europe” GmbH), obtained from coconuts, in symmetric supercapacitors by using lithium and sodium organic electrolytes. It is found that YP-50F delivers higher energy density when a lithium electrolyte containing LiBF₄ salt is employed. This electrolyte is chemically inert toward YP-50F. The most aggressive electrolyte toward YP-50F is LiPF₆-based electrolyte, which determines the lower energy and power densities. The interaction of LiBF₄- and LiPF₆-based electrolytes with functional groups results in the enrichment of the electrode surface with hydroxyl/epoxide and carbonyl groups. For the sake of comparison, in basic alkaline electrolyte, the carboxylic groups dominate the electrode surface (Karamanova et al., 2019, 2020). The sodium electrolyte with NaPF₆ salt is less aggressive toward YP-50F than that of LiPF₆ salt, as a result of which a good capacitance performance is observed in the sodium electrolyte. The results obtained are a good prerequisite for future research and for a more complete elucidation of the processes occurring in various organic electrolytes.

DATA AVAILABILITY STATEMENT

The raw data supporting the conclusions of this article will be made available by the authors, without undue reservation.

REFERENCES

- Bi, Z., Kong, Q., Cao, Y., Sun, G., Su, F., Wei, X., et al. (2019). Biomass-derived porous carbon materials with different dimensions for supercapacitor electrodes: a review. *J. Mater. Chem. A* 7, 16028–16045. doi: 10.1039/C9TA04436A
- Calvo, E. G., Rey-Raap, N., Arenillas, A., and Menéndez, J. A. (2014). The effect of the carbon surface chemistry and electrolyte pH on the energy storage of supercapacitors. *RSC Adv.* 4, 32398–32404. doi: 10.1039/C4RA04430D
- Chen, Z., Wang, X., Ding, Z., Wei, Q., Wang, Z., Yang, X., et al. (2019). Biomass-based hierarchical porous carbon for supercapacitors: effect of aqueous and organic electrolytes on the electrochemical performance. *ChemSusChem* 12, 5099–5110. doi: 10.1002/cssc.201902218
- Chmiola, J., Yushin, G., Gogotsi, Y., Portet, C., Simon, P., and Taberna, P. L. (2006). Anomalous increase in carbon capacitance at pore sizes less than 1 nanometer. *Science* 313, 1760–1763. doi: 10.1126/science.1132195
- Clark, D. T., and Dilks, A. (1979). ESCA applied to polymers. 23. RF glow discharge modification of polymers in pure oxygen and helium oxygen mixtures. *J. Polym. Sci. Polym. Chem.* 17, 957–976. doi: 10.1002/pol.1979.170170404
- Cresce, A. V. W., Russell, S., Borodin, O. A., Allen, J. L., Schroeder, M., Dai, M., et al. (2017). Solvation behavior of carbonate-based electrolytes in sodium ion batteries. *Phys. Chem. Chem. Phys.* 19, 574–586. doi: 10.1039/C6CP07215A
- Etacheri, V., Marom, R., Elazari, R., Salitra, G., and Aurbach, D. (2011). Challenges in the development of advanced Li-ion batteries: a review. *Energy Environ. Sci.* 4, 3243–3262. doi: 10.1039/C1EE01598B
- Fang, Y., Luo, B., Jia, Y., Li, X., Wang, B., Song, Q., et al. (2012). Renewing functionalized graphene as electrodes for high-performance supercapacitors. *Adv. Mater.* 24, 6348–6355. doi: 10.1002/adma.201202774
- Frackowiak, E., and Beguin, F. (2001). Carbon materials for the electrochemical storage of energy in capacitors. *Carbon* 39, 937–950. doi: 10.1016/S0008-6223(00)00183-4
- Hu, X., Deng, Z., Suo, J., and Pan, Z. (2009). A high rate, high capacity and long life (LiMn₂O₄ + AC)/Li₄Ti₅O₁₂ hybrid battery-supercapacitor. *J. Power Sources* 187, 635–639. doi: 10.1016/j.jpowsour.2008.11.033

AUTHOR CONTRIBUTIONS

BK carried out the main experiment and performed the electrochemical tests of the supercapacitor cells. MS, MG, and TS were involved in the experiments considering the *ex-situ* XPS analysis and CV characterization of YP-50F. AS and RS were involved in the discussion of the experimental results and the revision of the manuscript. BK, AS, and RS made the research plan and wrote the manuscript. AS provided the financial support. All authors contributed to the article and approved the submitted version.

FUNDING

This work was supported by the Bulgarian National Scientific Fund under project DFNI κII-06-OIIP04/5 and partially by the National Roadmap for research infrastructure 2017–2023 “Energy storage and hydrogen energetics (ESHER),” approved by DCM #354/29.08.2017.

ACKNOWLEDGMENTS

We would like to acknowledge Prof. Olya Stoilova (Institute of Polymers, Bulgarian Academy of Sciences) for the measurement of contact angles of YP-50F in organic and aqueous electrolytes.

- Hudak, N., and Huber, D. (2011). Nanostructured lithium-aluminum alloy electrodes for lithium-ion batteries. *ECS Trans.* 33, 1–13. doi: 10.1149/1.3557706
- Karamanova, B., Stoyanova, A., Shipochka, M., Girginov, C., and Stoyanova, R. (2019). On the cycling stability of biomass-derived carbons as electrodes in supercapacitors. *J. Alloys Compd.* 803, 882–890. doi: 10.1016/j.jallcom.2019.06.334
- Karamanova, B., Stoyanova, A., Shipochka, M., Veleva, S., and Stoyanova, R. (2020). Effect of alkaline-basic electrolytes on the capacitance performance of biomass-derived carbonaceous. *Materials* 13, 2941–2952. doi: 10.3390/ma13132941
- Kundu, S., Wang, Y. M., Xia, W., and Muhler, M. (2008). Thermal stability and reducibility of oxygen-containing functional groups on multiwalled carbon nanotube surfaces: a quantitative high-resolution XPS and TPD/TPR study. *J. Phys. Chem. C* 112, 16869–16878. doi: 10.1021/jp804413a
- Li, Q., Chen, J., Fan, L., Kong, X., and Lu, Y. (2016). Progress in electrolytes for rechargeable Li-based batteries and beyond. *Green Energy Environ.* 1, 18–42. doi: 10.1016/j.gee.2016.04.006
- Mak, W. F., Wee, G., Aravindan, V., Gupta, N., Mhaisalkar, S. G., and Madhavi, S. (2012). High-energy density asymmetric supercapacitor based on electrospun vanadium pentoxide and polyaniline nanofibers in aqueous electrolyte. *J. Electrochem. Soc.* 159, A1481–A1488.
- McDonough, J. K., Frolov, A. I., Presser, V., Niu, J., Miller, C. H., Ubieto, T., et al. (2012). Influence of the structure of carbon onions on their electrochemical performance in supercapacitor electrodes. *Carbon* 50, 3298–3309. doi: 10.1016/j.carbon.2011.12.022
- Metzger, M., Walke, P., Solchenbach, S., Salitra, G., Aurbach, D., and Gasteiger, H. A. (2020). Evaluating the high-voltage stability of conductive carbon and ethylene carbonate with various lithium salts. *J. Electrochem. Soc.* 167:160522. doi: 10.1149/1945-7111/abcabd
- Pasquier, A. D., Plitz, I., Gural, J., Badway, F., and Amatucci, G. G. (2004). Power-ion battery: bridging the gap between Li-ion and supercapacitor chemistries. *J. Power Sources* 136, 160–170. doi: 10.1016/j.jpowsour.2004.05.023

- Pazhamalai, P., Krishnamoorthy, K., Manoharan, S., and Kim, S. J. (2019). High energy symmetric supercapacitor based on mechanically delaminated few-layered MoS₂ sheets in organic electrolyte. *J. Alloys Compd.* 771, 803–809. doi: 10.1016/j.jallcom.2018.08.203
- Phattharasupakun, N., Wutthiprom, J., Suktha, P., Iamprasertkun, P., Chanlek, N., Shepherd, C., et al. (2017). High-performance supercapacitors of carboxylate-modified hollow carbon nanospheres coated on flexible carbon fibre paper: effects of oxygen-containing group contents, electrolytes and operating temperature. *Electrochim. Acta* 238, 64–73. doi: 10.1016/j.electacta.2017.03.208
- Ponrouch, A., Monti, D., Boschini, A., Steen, B., Johansson, P., and Palacin, M. R. (2015). Non-aqueous electrolytes for sodium-ion batteries. *J. Mater. Chem. A* 3, 22–42. doi: 10.1039/C4TA04428B
- Qian, W. J., Sun, F. X., Xu, Y. H., Qiu, L. H., Liu, C. H., Wang, S. D., et al. (2014). Human hair-derived carbon flakes for electrochemical supercapacitors. *Energy Environ. Sci.* 7, 379–386. doi: 10.1039/C3EE43111H
- Rufford, T. E., Hulicova-Jurcakova, D., Zhu, Z., and Lu, G. Q. (2008). Nanoporous carbon electrode from waste from waste coffee beans for high performance supercapacitors. *Electrochem. Commun.* 10, 1594–1597. doi: 10.1016/j.elecom.2008.08.022
- Simon, P., and Gogotsi, Y. (2008). Materials for electrochemical capacitors. *Nat. Mater.* 7, 845–854. doi: 10.1038/nmat2297
- Vali, R., Laheear, A., Janes, A., and Lust, E. (2014). Characteristics of non-aqueous quaternary solvent mixture and Na-salts based supercapacitor electrolytes in a wide temperature range. *Electrochim. Acta* 121, 294–300. doi: 10.1016/j.electacta.2013.12.149
- Wang, G. P., Zhang, L., and Zhang, J. J. (2012). A review of electrode materials for electrochemical supercapacitors. *Chem. Soc. Rev.* 41, 797–828. doi: 10.1039/C1CS15060J
- Wang, H., Liu, J., Zhang, K., Peng, H., and Li, G. (2015). Meso/microporous nitrogen-containing carbon nanofibers with enhanced electrochemical capacitance performances. *Synth. Met.* 203, 149–155. doi: 10.1016/j.synthmet.2015.02.013
- Wang, T., Zhang, S., Yan, X., Lyu, M., Wang, Bell, J., et al. (2017). 2-Methylimidazole-derived Ni-Co layered double hydroxide nanosheets as high rate capability and high energy density storage material in hybrid supercapacitors. *ACS Appl. Mater. Interfaces* 9, 15510–15524. doi: 10.1021/acsami.7b02987
- Yang, C. M., Kim, Y. J., Endo, M., Kanoh, H., Yudasaka, M., Iijima, S., et al. (2007). Nanowindow-regulated specific capacitance of supercapacitor electrodes of single-wall carbon nanohorns. *Am. Chem. Soc.* 129, 20–21. doi: 10.1021/ja065501k
- Yue, Z., Dunya, H., Ashuri, M., Kucuk, K., Aryal, S., Antonov, S., et al. (2020). Synthesis of a very high specific surface area active carbon and its electrical double-layer capacitor properties in organic electrolytes. *ChemEngineering* 4:43. doi: 10.3390/chemengineering4030043
- Zhong, C., Deng, G., Hu, H., Qiao, J., Zhang, L., and Zhang, J. (2015). A review of electrolyte materials and compositions for electrochemical supercapacitors. *Chem. Soc. Rev.* 44, 7484–7539. doi: 10.1039/C5CS00303B

Conflict of Interest: The authors declare that the research was conducted in the absence of any commercial or financial relationships that could be construed as a potential conflict of interest.

Copyright © 2021 Karamanova, Shipochka, Georgiev, Stankulov, Stoyanova and Stoyanova. This is an open-access article distributed under the terms of the Creative Commons Attribution License (CC BY). The use, distribution or reproduction in other forums is permitted, provided the original author(s) and the copyright owner(s) are credited and that the original publication in this journal is cited, in accordance with accepted academic practice. No use, distribution or reproduction is permitted which does not comply with these terms.